

# Real-time birefringence measurement with digital holographic microscopy

Tristan Colomb<sup>a,b</sup>, Florian Charrière<sup>b</sup>, Jonas Kühn<sup>b</sup>, Yves Bellouard<sup>c</sup>,  
Christian Depeursinge<sup>b</sup>

<sup>a</sup>Centre de Neurosciences Psychiatriques, Département de psychiatrie DP-CHUV, Site de Cery,  
1008 Prilly- Lausanne, Switzerland.

<sup>b</sup>Ecole polytechnique fédérale de Lausanne, Institute of imaging and applied optics, CH-1015  
Lausanne, Switzerland.

<sup>c</sup>Micro- & Nano- Scale Eng., Mechanical Eng. Dept, Eindhoven University of Technology, PO  
Box 513, 5600 MB Eindhoven, The Netherlands.

**Abstract:** Digital holographic microscopes using two orthogonal polarized reference waves provides real-time polariscopes. Birefringence induced by internal stress is imaged in optical fibers and in fused silica substrates, where lines are written with low-energy femtosecond pulses.

© 2007 Optical Society of America

**OCIS codes:** (090.1760) Computer holography; (120.5410) Polarimetry; (110.0180) Microscopy

## 1. Introduction

Digital holographic microscopes (DHM) are instruments that allow real-time measurements of the amplitude and phase of an optical wave reflected by or transmitted through a specimen [1]. A digital hologram, resulting from the interference between a reference and an object wave, is recorded in off-axis geometry on a CCD camera [2] and then, numerically processed to reconstruct the digital replica of the object wave [3]. In common practice, the physical reference wave and object wave have the same polarization to provide the best fringes contrast. Our approach is first to use two different reference waves orthogonally polarized and with different propagation directions (linear polarization oriented at 0 and 90 degrees) and second, to illuminate a specimen with a 45 degrees oriented linear polarized wave [4–6]. The obtained hologram contains now two different fringes patterns corresponding respectively to the interference between the object wave and the two reference waves. In other words, the polarization components of the object wave are projected on the orthogonal basis defined by the orthogonal reference waves. Because of different propagation directions of these references waves, the different orders of the polarization components can be selected in the Fourier domain by spatial filtering. A digital reconstruction of the two wavefronts is done using the Fresnel propagation in the convolution formalism [3], combined with a digital superposition of the wavefronts and a compensation for optical aberrations. This allows us to compute the polarization state of the Jones vector corresponding to the object wave and in particular to extract the birefringence properties of the specimen from the phase difference information. The main advantage of a two reference waves approach compared to common practice (i.e. using one reference wave and changing its polarization state [7]), is the possibility to record and to measure polarization state in real-time as all polarization information is simultaneously acquired.

## 2. Setup and reconstruction

The setup used is presented on Fig. 1(a). The Jones formalism allows us to write the orthogonal polarized reference waves as  $\mathbf{R}_1 = (r_1, 0, 0)$  and  $\mathbf{R}_2 = (0, r_2, 0)$  and the object wave  $\mathbf{O} = \exp[i\phi_O] (o_1, o_2, 0)$ , where  $\phi_O$  is the specimen optical path length seen by a linear polarized wave oriented at 0 degree and  $\Delta\phi_0 = \arg(o_2 - o_1)$  is the phase difference. The object and reference waves interfere in off-axis geometry on the CCD camera [Inset of Fig. 1(a)] to produce the digital hologram  $I_H = \mathbf{R}_1^2 + \mathbf{R}_2^2 + \mathbf{O}^2 + \mathbf{R}_1^* \mathbf{O} + \mathbf{R}_1 \mathbf{O}^* + \mathbf{R}_2^* \mathbf{O} + \mathbf{R}_2 \mathbf{O}^*$  [Fig. 1(b)].

Two wavefronts ( $\Psi_1$  and  $\Psi_2$ ) are now reconstructed in the Fresnel approximation by using the convolution formalism [3]:

$$\Psi_i(m, n) = NL_i^I(m, n) \cdot A \cdot \text{FFT}^{-1} \left\{ \text{FFT} [NL_i^H(k, l) I_{Hi}^F(k, l)] \cdot \exp[-i\pi\lambda d(\nu_k^2 + \nu_l^2)] \right\}, \quad (1)$$

where  $i = 1, 2$ , FFT is the Fast Fourier Transform;  $m, n, k, l$  are integers ( $-N/2 < m, n, k, l \leq N/2$ );  $d$ , the reconstruction distance;  $A = \exp(i2\pi d/\lambda)/(i\lambda d)$ ;  $\lambda$ , the wavelength;  $\nu_k = k/(N\Delta x)$ ,  $\nu_l = l/(N\Delta y)$  are the spatial

frequencies coordinates,  $NL_i^P$  are defined in the hologram ( $P = H$ ) or image ( $P = I$ ) plane and are used to compensate for aberrations. Instead of propagating the digital hologram  $I_H$ , we propagate two different filtered apodized holograms

$$I_{Hi}^F = \text{FFT}^{-1}[\text{FFT}(I_H \cdot AP)FM_i], \quad (2)$$

where  $AP$  is a numerical amplitude filter used to apodize the hologram and therefore to suppress numerical diffraction created by the finite window of the hologram (see Ref. [8] for details);  $FM_i$  is a numerical mask filtering the hologram to propagate only the real ( $\mathbf{RO}_i^*$ ) or the virtual ( $\mathbf{R}_i^*\mathbf{O}$ ) image.  $FM_i$  can be seen as a numerical pinhole with any shape definition [9]: in Fig. 1(c), the white rectangles define the selected spatial frequency areas corresponding to virtual images for each interference.

The numerical lenses  $NL_i^P$  are complex arrays with constant amplitude.  $NL_i^H$  is defined as a standard polynomial model [10] (other models are possible, as Zernike polynomials [3]):

$$NL_i(k, l) = \exp \left[ -i \frac{2\pi}{\lambda} \sum_{\alpha+\beta=o} P_{\alpha\beta} \cdot k^\alpha l^\beta \right], \quad (3)$$

where  $P_{\alpha\beta}$  are the NL parameters and  $o$  is the polynomial order. These parameters can be computed automatically by fitting the assumed flat areas in the reconstructed phase image with the NL model [3, 10] or by using a conjugated reference hologram [11]. Usually, in digital holography  $NL_i^H$  is written only to a digital reference wave  $R_{Di}(k, l)$  assumed to be a plane wave [1, 7], that corresponds to an order  $o = 1$ .

The  $NL_i^H$  have a great advantage for polarization imaging by using two different polarized reference waves. Indeed, as explained by Yokota *et al.* in Ref. [7], using two references involves that the reconstructed images are not in the same position in the reconstructed plane; therefore a coordinate transformation had to be applied as in Ref. [4] to compare the two wavefronts  $\Psi_i$ . By using this automated adjusted  $NL_i^H$ , the tilt introduced by the off-axis geometry is suppressed in the hologram plane and the reconstructed wavefronts are superposed with sub-pixel precision (see Ref. [3] for details). Furthermore, different aberrations of curvature in the two references waves can be compensated by using higher polynomial order for the numerical lenses definition.

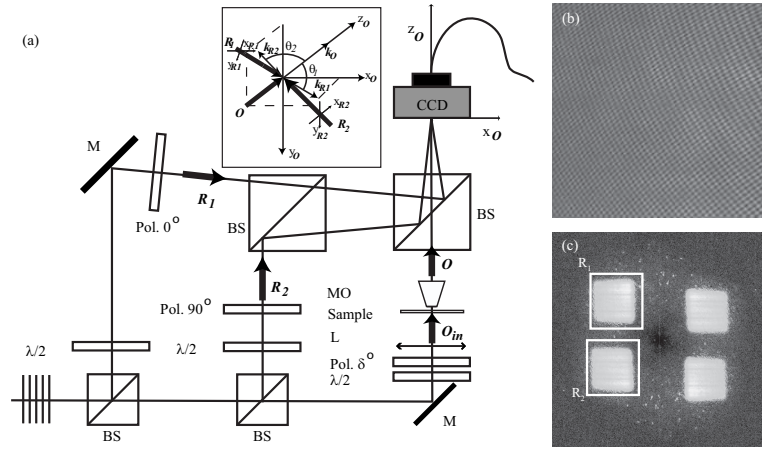


Fig. 1. (a) DHM setup for polarization imaging:  $\mathbf{O}$ , object wave;  $\mathbf{R}_i$ , the reference waves; M, mirrors; BS, beam splitter;  $\lambda/2$ , half wave plate; Pol., polarizers. Inset: off-axis geometry. (b) Portion of the digital hologram recorded with an optical fiber as specimen. (c) Spectrum of (b), rectangles delineating the frequency areas selected for defining the two filtered holograms  $I_{Hi}^F$ .

### 3. Results

Figure 2(a,b) present the two reconstructed images obtained from the filtered hologram  $I_{Hi}^F$ . Because of the use of the numerical lenses, the superposition has a sub-pixel precision. The subtraction pixel by pixel of these two images produces the phase difference image [Fig. 2(c)] that reveals the birefringence of the optical fiber and therefore the internal stress variations. Figure 3 presents the phase difference induced by a single line written in a long slab of fused silica using a femtosecond laser. The graph plots the mean phase difference along the vertical axis. From this measurement, the distribution of internal stress can be observed and the corresponding birefringence estimated (assuming that birefringence in this case only results from the presence of internal stress) [12].

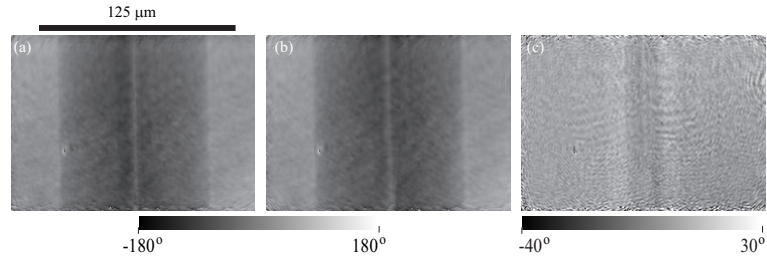


Fig. 2. (a) and (b) are the reconstructed phase image obtained from the filtered hologram  $I_{H1}^F$  and  $I_{H2}^F$  defined by the areas selected in Fig. 1(c). (c) is the phase difference image obtained by the subtraction (b)-(a).

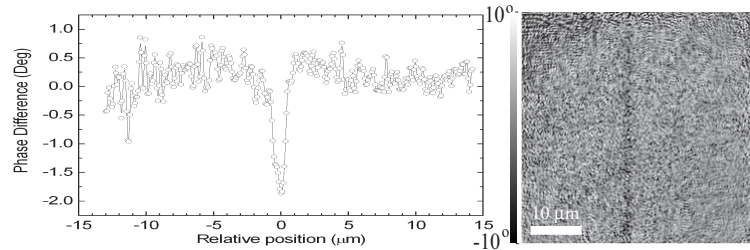


Fig. 3. Measurement of the phase difference along a line perpendicular to a single laser track. The phase difference graph is obtained by taking the mean phase difference along horizontal direction.

#### 4. Conclusion

In this paper, we demonstrate that the birefringence properties of a specimen can be imaged and measured using a single digital hologram recording. The use of numerical lenses makes the method user-friendly as wavefronts superposition is done automatically. Digital holography using two polarized reference waves is therefore an ideal technique to image and measure in real-time the birefringence properties of a specimen.

The authors are thankful of the Swiss National Science Foundation for supporting part of this work (research grant 205320-103885/1) and of the company Lyncée tec ([www.lynceetec.com](http://www.lynceetec.com)) for its fruitful collaboration.

#### References

1. E. Cuhe, P. Marquet, and C. Depeursinge, "Simultaneous amplitude-contrast and quantitative phase-contrast microscopy by numerical reconstruction of Fresnel off-axis holograms," *Appl. Opt.* **38**, 6994–7001 (1999).
2. U. Schnars and W. Jüptner, "Direct Recording of Holograms by a Ccd Target and Numerical Reconstruction," *Appl. Opt.* **33**, 179–181 (1994).
3. T. Colomb, F. Montfort, J. Kühn, N. Aspert, E. Cuhe, A. Marian, F. Charrière, S. Bourquin, P. Marquet, and C. Depeursinge, "Numerical parametric lens for shifting, magnification and complete aberration compensation in digital holographic microscopy," *J. Opt. Soc. Am. A* **23**, 3177–3190 (2006).
4. T. Colomb, P. Dahlgren, D. Beghuin, E. Cuhe, P. Marquet, and C. Depeursinge, "Polarization imaging by use of digital holography," *Appl. Opt.* **41**, 27–37 (2002).
5. T. Colomb, E. Cuhe, F. Montfort, P. Marquet, and C. Depeursinge, "Jones vector imaging by use of digital holography: simulation and experimentation," *Opt. Commun.* **231**, 137–147 (2004).
6. T. Colomb, F. Dürr, E. Cuhe, P. Marquet, H. Limberger, R.-P. Salathé, and C. Depeursinge, "Polarization microscopy by use of digital holography: application to optical fiber birefringence measurements," *Appl. Opt.* **44**, 4461–4469 (2005).
7. M. Yokota, Y. Terui, and I. Yamaguchi, "Analysis of polarization state by digital holography with polarization modulation," *Optical Review* **13**, 405–409 (2006).
8. E. Cuhe, P. Marquet, and C. Depeursinge, "Aperture apodization using cubic spline interpolation: application in digital holographic microscopy," *Opt. Commun.* **182**, 59–69 (2000).
9. E. Cuhe, P. Marquet, and C. Depeursinge, "Spatial filtering for zero-order and twin-image elimination in digital off-axis holography," *Appl. Opt.* **39**, 4070–4075 (2000).
10. T. Colomb, E. Cuhe, F. Charrière, J. Kühn, N. Aspert, F. Montfort, P. Marquet, and C. Depeursinge, "Automatic procedure for aberration compensation in digital holographic microscopy and applications to specimen shape compensation," *Appl. Opt.* **45**, 851–863 (2006).
11. T. Colomb, J. Kühn, F. Charrière, C. Depeursinge, P. Marquet, and N. Aspert, "Total aberrations compensation in digital holographic microscopy with a reference conjugated hologram," *Opt. Express* **14**, 4300–4306 (2006).
12. Y. Bellouard, T. Colomb, C. Depeursinge, M. Dugan, A. A. Said, and P. Bado, "Nanoindentation and birefringence measurements on fused silica specimen exposed to low-energy femtosecond pulses," *Opt. Express* **14**, 8360–8366 (2006).